Inferring carbon monoxide pollution changes from space-based observations

Drew T. Shindell
NASA Goddard Institute for Space Studies, New York, New York, USA
Center for Climate Systems Research, Columbia University, New York, New York, USA

Greg Faluvegi
Center for Climate Systems Research, Columbia University, New York, New York, USA

Louisa K. Emmons
National Center for Atmospheric Research, Boulder, Colorado, USA

Received 26 April 2005; revised 25 August 2005; accepted 23 September 2005; published 3 December 2005.

[1] We compare space-based measurements of carbon monoxide (CO) during April 1994 and October 1984 and 1994 from the early MAPS instrument with those during 2000–2004 from the MOPITT instrument. We show that a three-dimensional global composition model can be used to account for differences in retrieval sensitivity between the two instruments and between the different years of MOPITT data. This allows direct comparison of CO amounts over most of the globe at different times. These types of changes in short-lived constituents cannot be assessed with local measurements. Though the existing space-based data are too sparse both temporally and geographically to allow trend estimates, we find substantial variations in midtropospheric CO between the different years in many continental-scale regions. During April, average CO is ~12–18 ppbv (~10–20%) greater during 2000–2004 than during 1994 over North America, southeast Asia and North Africa though the global mean value is nearly the same. During October 1994, observations show CO enhancements of 15–20 ppbv relative to 1984 or 2000–2004 over South America and a similar, though slightly smaller (9–19 ppbv), enhancement globally. Southeast Asia, Europe and North America all show similar October CO levels in 1994 and 2000–2004, with both times showing substantially more pollution (13–29 ppbv) than 1984. Variations over Europe and Africa are consistent in both seasons, while changes elsewhere are not. Changes over southeast Asia and North Africa are substantially in excess of interannual variability, while those over North and South America and southern Africa are only marginally so. Model sensitivity studies examining the response to changes in emissions indicate probable causes of the CO changes over different regions. Over southeast Asia and North America, CO is most sensitive to industrial and biomass burning emissions, implying that changes in these sources likely account for the 13–29 ppbv increases seen there between 2000–2004 and earlier years. Over North Africa, CO is strongly influenced by numerous sources as well as meteorology, precluding attribution of increases to particular factors. Over South America and southern Africa, variations in both biomass burning and isoprene emissions likely contributed to the ~10–20 ppbv changes.

Citation: Shindell, D. T., G. Faluvegi, and L. K. Emmons (2005), Inferring carbon monoxide pollution changes from space-based observations, *J. Geophys. Res.*, *110*, D23303, doi:10.1029/2005JD006132.

1. Introduction

[2] Earth orbiting instruments have provided a unique, near-global view of many atmospheric trace gases, especially in the stratosphere. In the troposphere, however, where measurements are more challenging, carbon monoxide (CO) is the only pollutant to have been observed prior to the late 1990s. The Measurement of Air Pollution from Satellites (MAPS) instrument observed CO on Space Shuttle flights in 1984 and 1994. More recently, the Measurements of Pollution in the Troposphere (MOPITT) instrument on the Terra satellite has been observing CO since 2000. While the temporal coverage is thus quite limited, comparison between these CO observations could potentially provide useful information about changes during

0148-0227/05/2005JD006132$09.00

these three decades. Such a comparison is complicated, however, by the fact that the two instruments sample the vertical distribution of CO differently. We must therefore use an atmospheric chemistry model to interpret and compare the two sets of observations.

[3] We compare the space-based data sets using the NASA Goddard Institute for Space Studies (GISS) composition and climate model (containing representations of chemistry, aerosols, and climate). We first describe the observations (section 2) and the model (section 3). Following evaluation of the model's CO simulation (sections 3.2 and 3.3), we use the model results to calculate the difference between CO that the MAPS and MOPITT instruments would observe were they to view the same atmosphere, the sampling difference or "viewing difference" between the instruments (section 4.1). Quantification of this viewing difference allows us to directly compare the 1984, 1994 and 2000–2004 measurements. We also evaluate the viewing difference between MOPITT phase 1 and phase 2 observations, and the interannual variability during the 5 years of MOPITT measurements (section 4.2). Though there are insufficient data to establish long-term trends, a continental-scale regional analysis reveals substantial differences between the CO measured during the different decades over many parts of the world (section 4.3). These differences are then compared with the results of a series of sensitivity studies performed with the model to examine the response to various CO emissions changes and meteorology changes (section 5). This allows us to identify likely causes of the observed variations in CO abundance in each region. We conclude with a discussion of the implications of the results and potential for future studies using models to enhance the value of long-term pollutant monitoring from spaces (section 6).

2. Observations

[4] Measurements were made from the MAPS instrument for 10-day periods during October 1984, April 1994 and October 1994 [*Connors et al.*, 1999]. Though of relatively short duration, they likely provide a representative picture of the monthly mean value for those years since the lifetime of CO is relatively long (~1 month in the middle troposphere). While the orbital path and cloud cover prevented complete coverage, the measurements offer fairly good coverage over the 60°S–60°N range. All data discussed in this paper consist of averages over the entire 10-day measurement period during each month on a 5° by 5° grid. Comparison with correlative aircraft observations show biases of ~±10% (MAPS is ~2% low in the 1984 data, and ~10% high in the 1994 data) [*Connors et al.*, 1999; *Reichle et al.*, 1999].

[5] We use data from the MOPITT instrument for the period from April 2000 through April 2001, the so-called phase 1 retrievals, and from September 2001 to December 2004, the phase 2 retrievals [*Emmons et al.*, 2004]. In between these times, a break occurred in the record because of a cooler failure, which led to a different instrument configuration during the second phase. We use monthly mean values throughout this paper derived from version 3 retrievals. These data are gridded at a resolution of 1° by 1°, though we average over the model's 4° by 5° grid or the coarser MAPS grid for comparison. On the basis of a detailed evaluation against aircraft observations, mean biases range from about 7% in the lower troposphere to 3% in the upper troposphere, with the largest biases occurring over clean locations [*Emmons et al.*, 2004]. We therefore focus our regional analysis on continental sites, where we are most interested in the effects of pollution in any case.

[6] While both MAPS and MOPITT measure radiances in the thermal infrared, the differences in the instruments and retrieval algorithms result in differences in the vertical resolution of the retrieved CO mixing ratios. The sensitivity of the retrievals to the true atmospheric profile is described by averaging kernels. The vertical sensitivity of the MAPS retrieval is centered around 300–400 hPa, with a fairly broad averaging kernel that is globally uniform [*Reichle et al.*, 1999]. MAPS retrievals are weighted by the local number density profile, which gives them a shape peaking closer to 500 hPa, and a slight geographic variation (Figure 1). Sensitivity is very low in the 2 km nearest the surface. The MAPS retrievals are related to the true CO profile ($\mathbf{x}$) using the vertical averaging kernel ($\mathbf{A}$) by:

$$x_{MAPS} = \mathbf{A}\,\mathbf{x} \tag{1}$$

[7] The MOPITT retrievals incorporate a priori information [*Deeter et al.*, 2003]. The averaging kernels ($\mathbf{A}$) indicate the relative weighting between the a priori ($\mathbf{x_a}$) and true CO profiles ($\mathbf{x}$):

$$x_{MOP} = \mathbf{A}\,\mathbf{x} + (\mathbf{I} - \mathbf{A})\mathbf{x_a} \tag{2}$$

[8] While seven retrieval levels are reported, the MOPITT profiles typically have only 1 to 2 independent points (degrees of freedom) [*Deeter et al.*, 2004]. The 500 hPa retrieval level typically has a broad shape that most closely resembles the MAPS averaging kernel, while the 350 hPa retrieval level also looks similar in many places, though the kernels vary from location to location (Figure 1). However, given that the kernels from the two instruments represent different quantities and therefore are used differently to derive CO (equations (1) and (2)), they are not directly comparable. We make use of both the 350 and 500 hPa MOPITT levels here, as well as the 850 hPa level peaking closer to the surface. As with MAPS, the MOPITT instrument has very low sensitivity in the lowest few kilometers above the surface. However, unlike MAPS, the MOPITT averaging kernels depend upon surface emissivity and temperature, and therefore vary in space and time. It is therefore not possible to directly compare measurements from the two instruments. We instead use a chemistry climate model sampled using the same averaging kernels (and a priori profiles in the case of MOPITT) as used in the retrievals from the instruments to characterize the differences and allow comparisons between the 1984, 1994 and 2000–2004 data sets. We concentrate on April and October, the only months for which MAPS data exist.

3. Composition and Climate Model

3.1. Model Description

[9] We use the GISS composition model incorporated within the new, state-of-the-art GISS ModelE/Model III

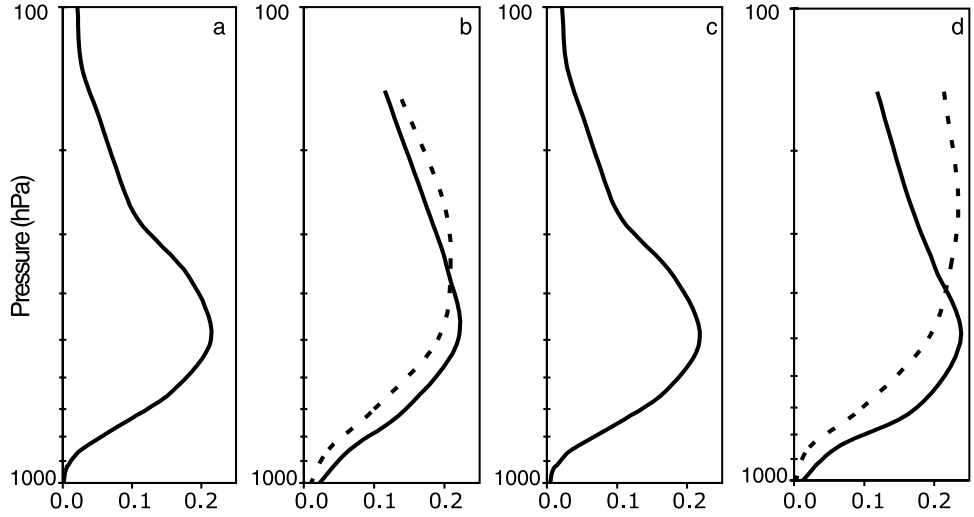

Figure 1. Averaging kernels from MAPS and MOPITT. Values are given at 37°E, 63°N for April for (a) MAPS and (b) MOPITT, and also for 10°E, 14°N for October for (c) MAPS and (d) MOPITT. The MAPS plots show the globally applicable kernel weighted by the local number density profile taken from the GCM. The MOPITT plots show the 350 hPa retrieval level (dotted) and the 500 hPa retrieval level kernels (solid) for 2000. These are fairly typical example points, though the MOPITT kernels can vary substantially in some areas [*Emmons et al.*, 2004]. MAPS kernels continue above 100 hPa but taper off very rapidly so that that region contributes little to the retrieved CO.

GCM [*Schmidt et al.*, 2005]. The model incorporates a tropospheric chemistry scheme that represents reactions between 32 gases, including basic HO_x-NO_x-O_x-CO-CH_4, along with isoprene, peroxyacetylnitrates and the lumped hydrocarbon families paraffins, alkyl nitrates, alkenes and aldehydes [*Shindell et al.*, 2003]. It contains complete sources and sinks for all emitted gases, including methane. The chemistry is fully coupled to the model's sulfate aerosol scheme, an update of [*Koch et al.*, 1999]. Both the chemistry and sulfate are fully interactive with the GCM so that soluble tracers are coupled to the hydrologic cycle, dry deposition is calculated according to surface winds, etc. The climate model includes substantial improvements to the physics compared with the earlier GISS model II′, especially in the convection and boundary layer modules. The model also incorporates a liquid tracer budget, allowing more realistic calculation of the fate of soluble species (which are otherwise arbitrarily returned to the gas phase if they are not removed by precipitation in a single time step). We ran the model at 4° by 5° resolution with 23 vertical layers, of which roughly 12–14 are within the troposphere. Composition is calculated from the surface to the meteorological tropopause.

[10] A control run was performed for 7 years, of which we use the average over the last 5 years. Meteorological fields were generated internally by the GCM using present-day (1990s) boundary conditions (sea surface temperatures, sea ice, greenhouse gases, volcanic aerosols, etc.). The control run used our base case emissions which are largely based on data sets from the Global Emissions Inventory Activity (GEIA) project [*Benkovitz et al.*, 1996] representing roughly 1990 emissions as detailed by *Shindell et al.* [2001].

[11] A suite of additional simulations was performed to examine the response to different emissions data sets and meteorology. The emissions included those from the EDGAR-3 1995 inventory [*Olivier and Berdowski*, 2001] and the Global Fire Emissions Database (GFED) [*Van der Werf et al.*, 2003], as given in Table 1. Altered meteorology was incorporated via "nudging" (i.e., linear relaxation) toward ERA-40 reanalyses for the MOPITT phase 1 observation period (2000–2001). We largely defer discussion of these sensitivity studies to section 5. However, during the following sections concerning comparison between the model and satellite observations, we will include some discussion of one of these runs that used nudging toward observed meteorology from 2000–2001, GFED 2000–2001 CO biomass burning emissions and EDGAR 1995 industrial emissions (which we therefore denote BB00/E95). This run was among the most different from the control, with generally larger emissions in the Southern Hemisphere (SH) and smaller emissions in the Northern Hemisphere (NH). Thus these two runs typically provide a reasonable estimate of the spread of model results.

3.2. Comparison With Surface and Sonde Data

[12] The chemical fields in the modelE control run are similar to those shown in our earlier model documentation

Table 1. Direct Carbon Monoxide Sources

Source	Tg/yr CO
GEIA industrial	498
GEIA biomass burning	490
EDGAR 95 industrial[a]	547
EDGAR 95 biomass burning	298
GFED 2000-1 biomass burning[b]	467

[a]EDGAR 1995 industrial emissions are the sum of the following sources: industrial (32), fossil fuel (264), waste handling (4), agricultural (16), and biofuel (231).

[b]The GFED value is based on May 2000 to April 2001. Using April 2000 to March 2001 instead gives 450 Tg/yr.

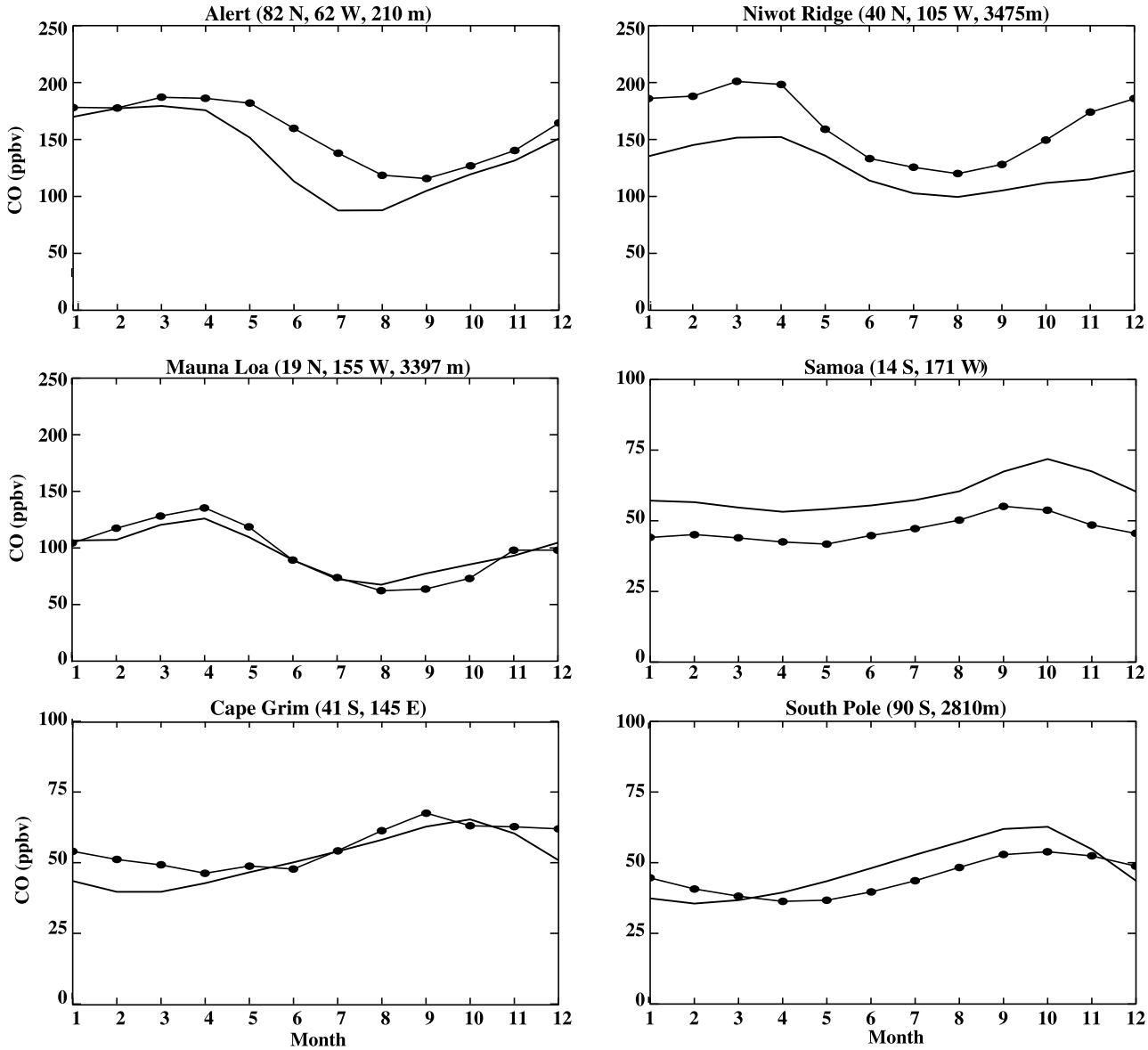

Figure 2. Comparison between the annual cycle of surface CO (ppbv) in the GCM (line with symbols) and in CMDL observations from the indicated sites (thick line). Observations are averages of all available 1990s data, covering 6–10 years for these stations. GCM results are 8-year averages from the control run. The average standard deviation in the monthly values for these 6 stations is 7 ppbv, with values up to 26 ppbv for individual stations and months.

paper [*Shindell et al.*, 2003], with some notable improvements. We have discussed this elsewhere [*Shindell et al.*, 2005], and a complete documentation of the new model including chemistry in both the troposphere and stratosphere is in preparation (the simulations described here do not include stratospheric chemistry). Briefly, we compared the annual cycle of surface CO in the model with measurements from the NOAA/Climate Monitoring and Diagnostics Laboratory (CMDL) network [*Novelli et al.*, 1998]. Results at representative sites are shown in Figure 2. Observations are averages over all available 1990s monthly mean data (6–10 years). The model does a very good job of capturing the seasonality of surface CO. Systematic biases exist at a few locations, however, such as the positive bias at Niwot Ridge and the negative bias at Samoa. Overall though, the model clearly captures both the annual cycle of CO and the variation in amount as a function of latitude (Figure 2 shows locations from 82°N to 90°S). Further evaluation of the model's CO distribution is presented in section 3.3.

[13] CO is strongly influenced by the abundance of OH, its main oxidizer, and of methane, whose oxidation is a large source of CO. The simulation of these gases is generally similar to the earlier model. The mass-weighted global mean OH is 9.6×10^5 molecules cm^{-3}, versus 9.7×10^5 molecules cm^{-3} in the previous version, both in good agreement with the $9.4 \pm 1.3 \times 10^5$ molecules cm^{-3} derived from observations [*Prinn et al.*, 2001]. The CH_4 interhemispheric gradient is again reproduced quite well, although a somewhat exaggerated CH_4 seasonality at high northern latitudes also persists in the new version. Given the

Table 2. Ozone Differences Between Models and Sondes[a]

Pressure Level, hPa	Average Difference Nine-Layer Model II′	Average Difference, 23-Layer Model II′	Average Difference, 23-Layer Model E	Average Bias, 23-Layer Model E	Standard Deviation of Observations
125	108.6 (29%)	83.7 (22%)	50.3 (13%)	3.9 (1%)	137
200	79.5 (39%)	44.9 (22%)	34.1 (17%)	−21.3 (10%)	74.2
300	15.1 (20%)	28.9 (39%)	17.8 (23%)	9.5 (13%)	32.2
500	9.3 (20%)	10.6 (23%)	6.5 (14%)	2.5 (5%)	11.4
900	9.3 (31%)	6.6 (22%)	5.6 (19%)	−1.4 (5%)	9.9
Average	(28%)	(26%)	(17%)	(7%)	...

[a]Differences are in ppbv. Comparisons are between the models and the 16 recommended sites of *Logan* [1999], having excluded the two sites with 4 months or less data. Average differences are from the month-by-month absolute value differences between the model and the sondes. Values in parentheses are percent difference with respect to observed values at these levels. The nine-layer model [*Shindell et al.*, 2001] did not include PANs and higher hydrocarbons. The "Average" row is the average of the five levels in the table. The sites are Resolute, Edmonton, Hohenpeissenberg, Sapporo, Boulder, Wallops Island, Tateno, Kagoshima, Naha, Hilo, Natal, Samoa, Pretoria, Aspendale, Lauder, and Syowa.

reasonable simulation of high-latitude CO, this appears to be a result of the prescribed methane emissions [*Fung et al.*, 1991] rather than biases in the seasonality of tropospheric oxidation.

[14] Ozone is the main source of OH radicals, and one of the only gases for which long-term tropospheric climatologies are available above the surface. Comparison of the simulated annual cycle of ozone to a balloon-sonde climatology shows a reduction in the average absolute value monthly mean difference from 26% to 17% (Table 2). The average monthly bias in modelE is only 7%. ModelE has eliminated the overly large wintertime downward ozone flux at high latitudes of the previous GCM while preserving the good agreement with ozone and precursor observations near the tropopause at lower latitudes [*Shindell et al.*, 2003] (Table 2). The stratosphere-to-troposphere O_3 flux is 477 Tg/yr across 150 hPa, in accord with the 450–590 Tg/yr range at 100 hPa estimated indirectly from satellite observations [*Gettelman et al.*, 1997].

3.3. Comparisons Between Model and Satellite CO Data

[15] To make proper comparisons between the model and satellite data, the vertical sensitivity of the retrievals must be taken into account by transforming the model CO profiles according to equations (1) and (2) (section 2). In the MAPS case, GCM output is regridded to 5° by 5° and the CO profiles scaled by the MAPS averaging kernel. In the MOPITT case, the 1° by 1° averaging kernels and the same a priori CO profiles used in creating the MOPITT retrievals are used to sample the larger GCM grid box containing that location and the results are then averaged over the model's 4° by 5° resolution. The results are not sensitive to whether the averaging is done before or after the model is sampled. Though the model's CO is a full diurnal average and the observations are averages over measurements taken at particular overpass times (during both day and night), this should have a negligible effect on the model/data comparison given the relatively long lifetime of CO. For simplicity and better comparison with the nudged sensitivity studies, we focus the comparisons with MOPITT on the phase 1 retrieval period.

[16] The CO spatial distributions in the model when sampled as MOPITT using the 500 hPa retrieval level averaging kernels and in observations from the same MOPITT level and from MAPS during April and October are illustrated in Figure 3. For model evaluation, we compare primarily with the more complete MOPITT data. Clearly the model is able to capture the broad seasonal changes between April and October and enhanced pollution levels over NH continents. The magnitude of maxima over tropical continental areas in October and midlatitude industrialized regions in April does not agree well with observations, however. Of course the control run used an emission inventory for ~1990, while the observations range from 1984 to 2001. Thus the control run would not be expected to match all the observations, as emissions vary on interannual and longer timescales (the influence of altered emissions will be explored in section 5).

[17] Though the magnitude of emissions from particular sources can vary greatly with time, the location of emissions from industry and to a lesser extent from biomass burning will have varied somewhat less over the decades of interest. We therefore believe that the spatial pattern is a useful validation of the model despite emissions differences from one year to another. Regression plots for model-MOPITT 500 hPa comparisons during April and October are shown in Figure 4. It is clear that while the overall correlation is quite good, the April control run fields are systematically low at CO values below about 100 ppbv, which encompasses most of the SH, and slightly too large at the greatest CO values, which occur primarily over polluted continental regions in the NH. During October, the range of values shrinks substantially, but again there is a tendency toward negative biases at low CO values and positive biases over the most polluted areas (Figure 4b). However, the model clearly underestimates the very large values (>120 ppbv) seen over SH continents. Unsurprisingly, CO in these regions is quite sensitive to biomass burning emissions, and the aforementioned BB00/E95 run including 2000–2001 biomass burning emissions is able to capture the October CO distribution much better (Figure 4d). This run also has a reduced bias over the remote SH, suggesting that the model's underestimate of CO in this area may stem at least in part from an underestimate of long-range transport from the continents. Correlations between the model and MAPS observations are somewhat less than for MOPITT, though statistically significant at the 99% level, with values of 0.90 for April 1994, 0.50 for October 1994, and 0.50 for October 1984 using the BB00/E95 simulation.

[18] The monthly regression coefficients between the control run and the MOPITT observations at several levels are shown in Table 3. Clearly the model does quite a good job of reproducing the spatial distribution of the measurements during most months and at levels throughout the troposphere. The correlations are statisti-

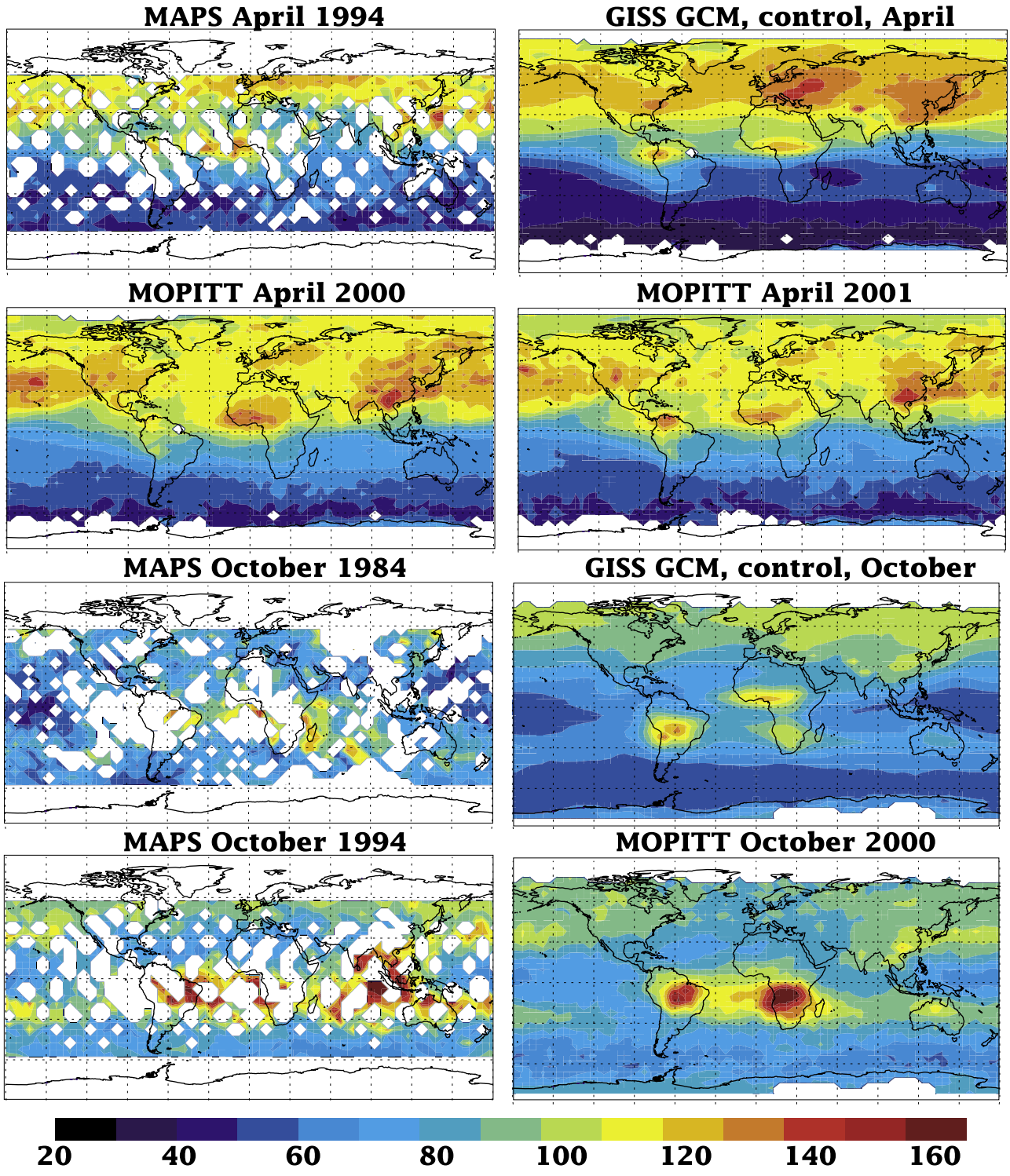

Figure 3. April and October distributions of CO (ppbv). MOPITT data are for the 500 hPa retrieval level. GCM plots show model output when sampled using the MOPITT 500 hPa averaging kernels for April 2000 and October 2000. Results for April simulations sampled with the April 2001 kernels are nearly identical. White areas indicate no data.

cally significant at the 99% confidence level during all months at all levels. R values are 0.89 or greater during the boreal winter and spring at all levels. Correlation values at the different vertical levels (850, 500, and 350 hPa) differ by 0.04 or less during all months (except June, when the difference is 0.07), indicating little variation in the fidelity of the simulation with height. The correlation is weakest during the biomass burning season. The last two columns of Table 3 give the monthly correlations and biases from the BB00/E95 run. This run, with greater SH biomass burning

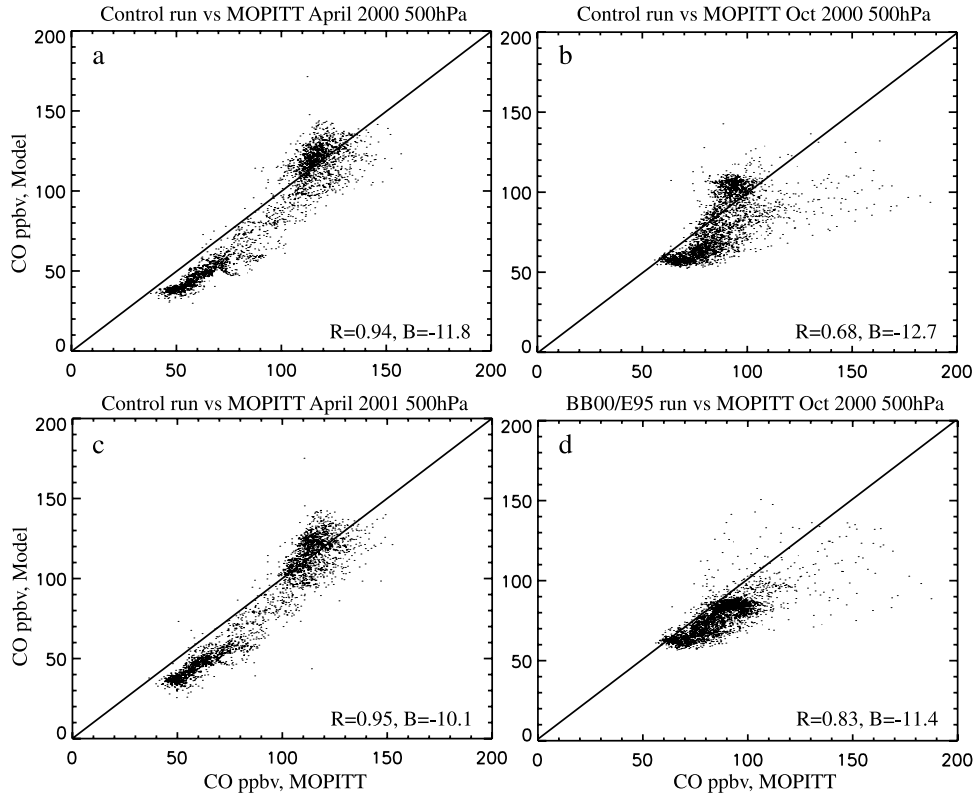

Figure 4. Correlation between CO in MOPITT 500 hPa retrieval level observations and in the GCM control run using the MOPITT sampling for (a) April 2000, (b) October 2000, and (c) April 2001. (d) Similar correlation for October 2000 using the BB00/E95 run. Values in the bottom right corner of each plot give the global correlation coefficient R and the global mean area-weighted bias B (GCM-MOPITT).

emissions, has substantially better correlations during September–November (as in Figure 4d). The correlations are somewhat worse during some boreal winter and spring months, however, so that the annual average is nearly unchanged. The similarity between these runs, with substantial differences in emissions, supports our contention that the spatial pattern is a relatively robust quantity for model validation despite emissions uncertainties.

[19] Global mean biases at the 500 and 350 hPa levels are within 1–2 ppbv of each other for all months, while the 850 hPa level has ~9–11 ppbv less CO than the other levels for the annual average, and is within 16 ppbv for individual months. The close agreement between the biases across pressure levels indicates that there are no substantial differences between systematic biases at different vertical levels other than a somewhat larger (though similar in percentage terms) bias near the surface where both instruments' averaging kernels become quite small. This is an important point for sampling the model with varying vertical averaging kernels. The model's global mean bias relative to

Table 3. Global Mean Regression and Biases Between Control Run (or BB00/E95 When Indicated) and MOPITT Data[a]

	R Value 850 hPa	Bias 850 hPa	R Value 500 hPa	Bias 500 hPa	R Value 350 hPa	Bias 350 hPa	R Value 500 hPa BB00/E95	Bias 500 hPa BB00/E95
April 2000	0.95	−19.8	0.94	−11.8	0.94	−10.4	0.96	−16.8
May 2000	0.93	−22.5	0.91	−14.9	0.89	−13.6	0.95	−18.5
June 2000	0.89	−19.6	0.86	−13.2	0.82	−12.1	0.90	−15.1
July 2000	0.82	−12.7	0.81	−10.1	0.78	−9.7	0.81	−9.9
Aug. 2000	0.80	−15.8	0.82	−9.8	0.81	−8.7	0.84	−10.1
Sep. 2000	0.74	−19.8	0.73	−12.3	0.73	−11.1	0.84	−11.8
Oct. 2000	0.71	−23.6	0.68	−12.7	0.68	−10.8	0.83	−11.4
Nov. 2000	0.81	−23.3	0.82	−11.1	0.82	−8.7	0.88	−10.9
Dec. 2000	0.89	−25.6	0.90	−10.6	0.91	−7.4	0.92	−8.7
Jan. 2001	0.90	−26.5	0.92	−10.8	0.93	−7.1	0.89	−9.8
Feb. 2001	0.90	−15.7	0.92	−6.1	0.92	−3.1	0.89	−9.1
March 2001	0.94	−15.5	0.95	−6.5	0.95	−3.9	0.90	−11.5
April 2001	0.94	−21.0	0.95	−10.1	0.95	−7.5	0.85	−11.7
Average	0.86	−20.1	0.86	−10.8	0.86	−8.8	0.88	−11.9

[a]Regression and biases are in ppbv. Biases are in the model with respect to observations and are area weighted.

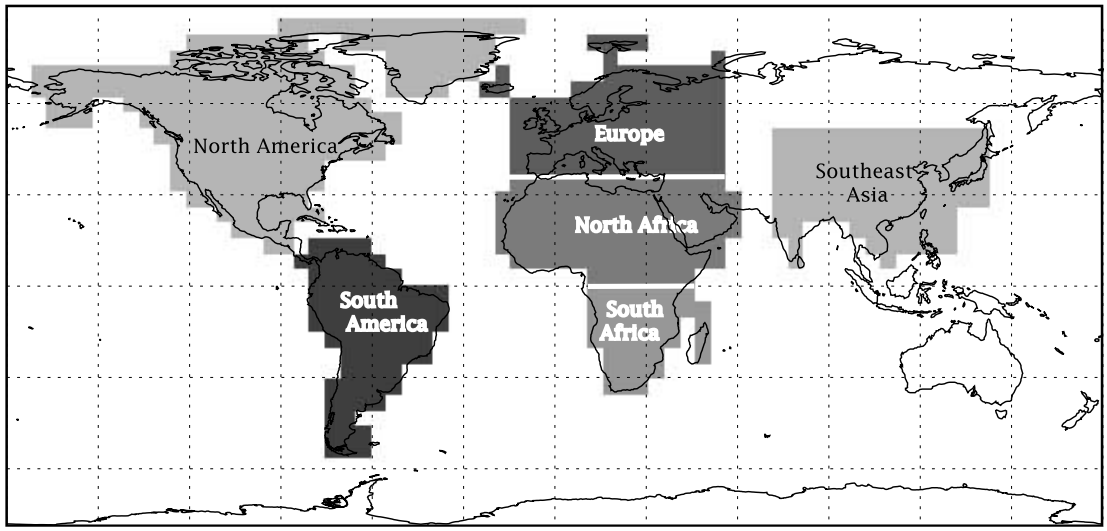

Figure 5. Definition of regions used in this study.

MOPITT observations is 1.4 ppbv larger at 500 than at 350 hPa for April 2000, but 2.6 ppbv larger for April 2001. This indicates that the difference between the model's biases at different levels is comparable to the range of interannual variability, again suggesting that differences between the shapes of the model's vertical CO profiles and the observations are relatively small, especially away from the surface. Biases show some seasonality, with smaller values during the boreal winter and larger values during the spring and the biomass burning season. The model's overall negative bias comes largely from the SH, where the GEIA emissions seem to be too small for 2000–2001 (discussed further in section 5). Biases in various NH regions are typically modest, and of either sign. For example, using the regions shown in Figure 5, the annual average biases at 850 hPa are less than 5 ppbv over North America and North Africa, with larger values of −19 ppbv over SE Asia and +24 ppbv over Europe. The positive European bias is eliminated by changing from the ~1990 GEIA emissions to the more recent EDGAR 1995 inventory (see section 5).

[20] We have also tested the model's ability to reproduce the observed vertical structure of CO by comparing the simulated ratio of the 850 to the 350 hPa retrieval level CO with that seen by MOPITT. Regionally averaged, the observed ratio lies between the values from the control

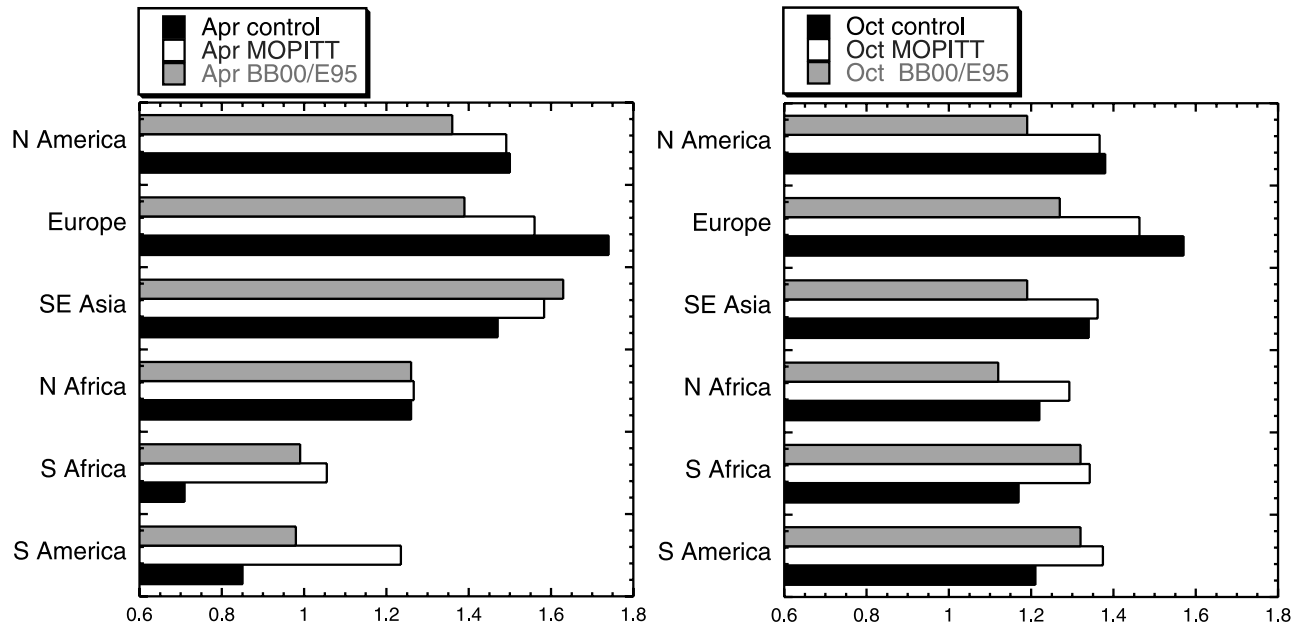

Figure 6. Ratio of 850 to 350 hPa retrieval level CO seen in MOPITT and in GCM simulations. Results are area-weighted averages over the indicated regions for (left) April and (right) October.

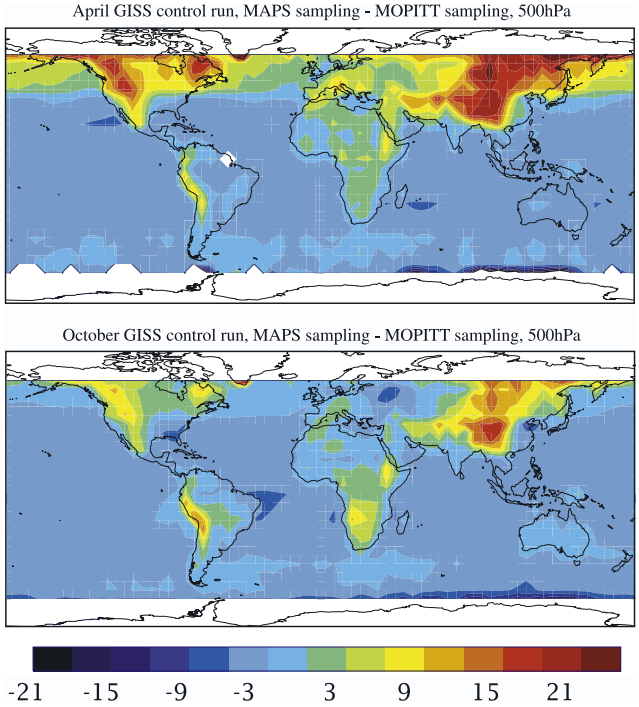

Figure 7. CO viewing difference (ppbv) between the space-based instruments calculated using the GCM control run sampled with the MAPS averaging kernel and the MOPITT 500 hPa 2000 averaging kernels for (top) April and (bottom) October. This quantity represents the difference between what the two instruments measure based only on the different retrieval sensitivities (i.e., were each to observe the identical atmosphere).

and BB00/E95 runs for the polluted regions of the NH during April and October, except for a very slight discrepancy over SE Asia during October (Figure 6). The ratios are also quite close for both northern and southern Africa, where they are within 0.07. The modeled ratios are too low, however, over South America, especially during April. This is the only case for which the difference between the model and the observations is larger than the spread of model values, suggesting that this discrepancy is not purely a function of emissions. Indeed our annual CO emissions from biomass burning over South America range from 73 Tg/yr in the EDGAR data set to 119 Tg/yr in the GFED, while recent inverse models yield results of 96–119 Tg/yr [*Arellano et al.*, 2004], 120–128 Tg/yr [*Pétron et al.*, 2002] and 58 Tg/yr [*Pétron et al.*, 2004]. This suggests that while our emissions may be on the low side, they are not greatly off. Instead, the model bias may be related to biases in the strength or location of convective activity in this region in the GCM, which has a large impact on the lower to upper tropospheric CO ratio [*Faluvegi et al.*, 1999]. The model clearly captures the general difference in the ratio between highly and less polluted regions and the seasonal cycle of larger values in the NH in April and in the SH in October.

[21] Overall, the comparisons with surface and satellite CO observations show that the model is able to capture the annual cycle and large-scale behavior of CO in the atmosphere, especially during the boreal winter and spring. Comparison with MOPITT soundings at several pressure levels, which have themselves been validated against aircraft profiles [*Emmons et al.*, 2004], and the ratio of lower to upper level CO shows that the model also captures the vertical structure of global CO relatively well and that for regional scales, biases are typically quite small. Thus, although the control simulation exhibits notable biases over local areas during some seasons, the model appears to reproduce observations well enough to allow it to be used to aid in the interpretation of the large-scale changes in CO observed from space.

4. Comparison Between MAPS and MOPITT

4.1. MOPITT/MAPS Viewing Difference

[22] Figure 3 shows sizable differences between the 1980s and 1990s MAPS observations and the more recent MOPITT 500 hPa retrieval level measurements. To accurately quantify these, we first compare artificial retrievals obtained from the model control run using the sampling of the two space-borne instruments (equations (1) and (2)). For the MOPITT sampling, we use the phase 1 averaging kernels and a priori CO profiles. The results are averaged to 5° by 5° for comparison with MAPS sampling. The resulting "viewing difference" is generally largest in regions with relatively high CO abundances (Figure 7). Not all areas with large abundances show large differences, however. For example, the greatest April 500 hPa MOPITT retrieval level CO values (140–150 ppbv) in the control run occur over Europe (Figure 3, top right), especially in the east, where the viewing difference is quite small (0–4 ppbv).

[23] Viewing differences are enhanced over areas with high surface albedo, such as the Himalayas, Rockies, Andes and Siberia during April. While the MAPS kernel is constant, the MOPITT kernel varies with surface emissivity, likely accounting for many of these features. Additionally, the MAPS kernel is applied directly to the model CO distribution, while the MOPITT transformation incorporates an a priori CO profile. An examination of the vertical structure of the CO retrievals using the two instruments' averaging kernels indicates that the differences are influenced by a number of factors, including the magnitude of a polluted layer of increased CO mixing ratios in the upper troposphere that is present in some regions and of course the differences in the shape of the two instruments' kernels, especially slight differences in the relatively weak sensitivity to the large CO abundances in the boundary layer.

[24] We believe that given the model's ability to reproduce surface observations of CO and the high correlation between the model's CO fields and MOPITT observations the model-based calculation of the MAPS versus MOPITT viewing difference is reasonable. Though the correlation with MOPITT clearly showed some systematic biases in the model control run (Figure 4), as discussed in the previous section, the effects of these will be minor as they will occur in both samplings. The viewing difference will be primarily sensitive to errors in the shape of the CO profile. Given that the correlation between the model and MOPITT is consistently high across the vertical range of MOPITT data (Table 3), it appears that the model captures the true CO

Table 4. Interannual Variations in MOPITT CO During 2000–2004[a]

Region	April Mean	April Maximum	October Mean	October Maximum
Global	2.5	6.2	4.3	10.7
N. America	3.2	9.9	2.0	12.5
S. America	3.8	8.2	1.4	10.2
Europe	1.8	5.7	7.8	17.3
N. Africa	4.4	9.0	4.1	6.7
S. Africa	1.2	3.8	3.7	10.0
SE Asia	3.2	7.8	9.4	15.3

[a]Variations are in ppbv. Values have been adjusted for averaging kernel differences from year to year using the viewing differences derived from the GCM control run. All quantities are absolute values based on the 5 years of 500 hPa retrieval level data.

profile's shape reasonably well. Global mean biases also are quite similar at the various vertical levels, as shown previously. This is true for regional biases as well, which generally vary less than the viewing differences shown in Figure 7. For example, the October bias over northern Africa is 1.6 ppbv at 850 hPa, 1.3 at 500 hPa and 2.8 ppbv at 350 hPa. Thus biases vary by less than 2 ppbv between levels, while the viewing difference is up to 18 ppbv. Similarly, April biases over North America are 8.2 ppbv at 850 hPa, 2.3 at 500 hPa, and 1.9 at 350 hPa. The variation is thus within 7 ppbv across levels, which will lead to a much smaller contribution to the viewing difference given the general similarity in the shape of the averaging kernels.

[25] To test the robustness of the model-derived viewing difference, we repeated the two sampling calculations using the BB00/E95 simulation. As a reminder, this run had altered emissions that were generally smaller in the NH and larger in the SH and used nudging toward observed meteorology leading to the somewhat different results shown previously (e.g., Figures 4d and 6 and Table 3). The viewing difference obtained from this run is quite similar to that shown in Figure 7. MAPS is smaller than MOPITT by 2.4 and 3.0 ppbv globally during April and October, respectively, using the BB00/E95 run as compared with 1.4 and 2.7 ppbv using the control run. Regionally, the area-weighted viewing differences calculated using the two simulations are within 3.5 ppbv for all the regions shown in Figure 5 during both April and October, and are in general much closer. Thus it appears that the viewing difference is remarkably robust.

[26] During October, MOPITT sampling yields more CO than MAPS sampling over Europe and North Africa, while in April, the situation is reversed. Thus the viewing difference is not an intuitively obvious quantity. Regionally, it ranges from 0.4 to 6.1 ppbv, the high end being substantial relative to regional mean CO values. It is therefore an important factor in comparing observations from the two instruments, and it is fortunate that it appears to be fairly robust to variations in emissions and meteorology. A similar calculation using the MOPITT 350 hPa retrieval level yields a substantially larger viewing difference, especially during April, indicating that the 500 hPa retrieval level is indeed the most appropriate for comparison with MAPS data. We note also that calculating the viewing difference using only grid points with coverage in the MAPS 1984 data set (the data set with the most limited spatial coverage) changes the regionally averaged values by less than 2.3 ppbv.

4.2. MOPITT Interannual Variability

[27] A similar sampling of the GCM using the MOPITT phase 2 averaging kernels was also performed. This allows us to characterize both the phase 1 versus phase 2 viewing difference and to use the viewing differences to allow comparison between MOPITT observations during different years. We find that both globally and regionally, the viewing difference between the phase 1 and phase 2 retrievals is quite small. During April, the viewing difference between the two phase 1 years is 0.5 ppbv or less for all regions, while the maximum difference within the phase 2 years is 0.7 ppbv. Between phase 1 and phase 2, this increases to a maximum of 2.8 ppbv over North America, and less than 1.5 ppbv in other regions and in the global mean. October viewing differences between the 5 years of observations show values less than 1.5 ppbv for all regions and for the global mean. Thus in general the viewing differences between the two phases are about a factor of four larger than between the years within a phase, but even those larger values are still fairly small and much smaller than the MAPS-to-MOPITT viewing differences.

[28] These viewing differences were then used to examine the interannual variability during the 5 years of MOPITT data. Since the instrument samples the atmosphere slightly differently each year, we calculated regionally averaged area-weighted differences between MOPITT 500 hPa retrieval level CO in different years adjusted using the control run viewing differences appropriate to each comparison (Table 4). Using our large regional averages, the April average year-to-year differences are less than 4.5 ppbv in all regions, with maximum interannual differences of about 10 ppbv. The variability is larger in October, with average interannual differences of up to 9.4 ppbv and maximum values over 10 ppbv in all regions (except North Africa) and in the global mean. This characterization of interannual variability provides a background against which to evaluate potential longer-term changes (e.g., related to fossil fuel usage, which has little interannual variability at regional scales).

4.3. Variations Between 1984, 1994 and 2000–2004

[29] Having calculated the viewing differences between the two instruments, we can then reasonably compare the MAPS and MOPITT data sets. We begin by calculating the difference between MOPITT phase 1 and MAPS CO accounting for the instruments' atmospheric sampling differences (Figure 8). We also show the MAPS 1994 versus 1984 difference. It is clear that many of the differences are quite large at small spatial scales. However, spatial coverage is fairly limited in some areas because of the MAPS data sets. We therefore concentrate on averages over the regions shown in Figure 5 for a more robust comparison. Additionally, we use the average values over the 5 years of MOPITT data calculated using the viewing differences between years to convert all years to equivalent 2000-sampling values. This allows comparison between MAPS and MOPITT averages using the viewing difference based on the MOPITT 2000 averaging kernels.

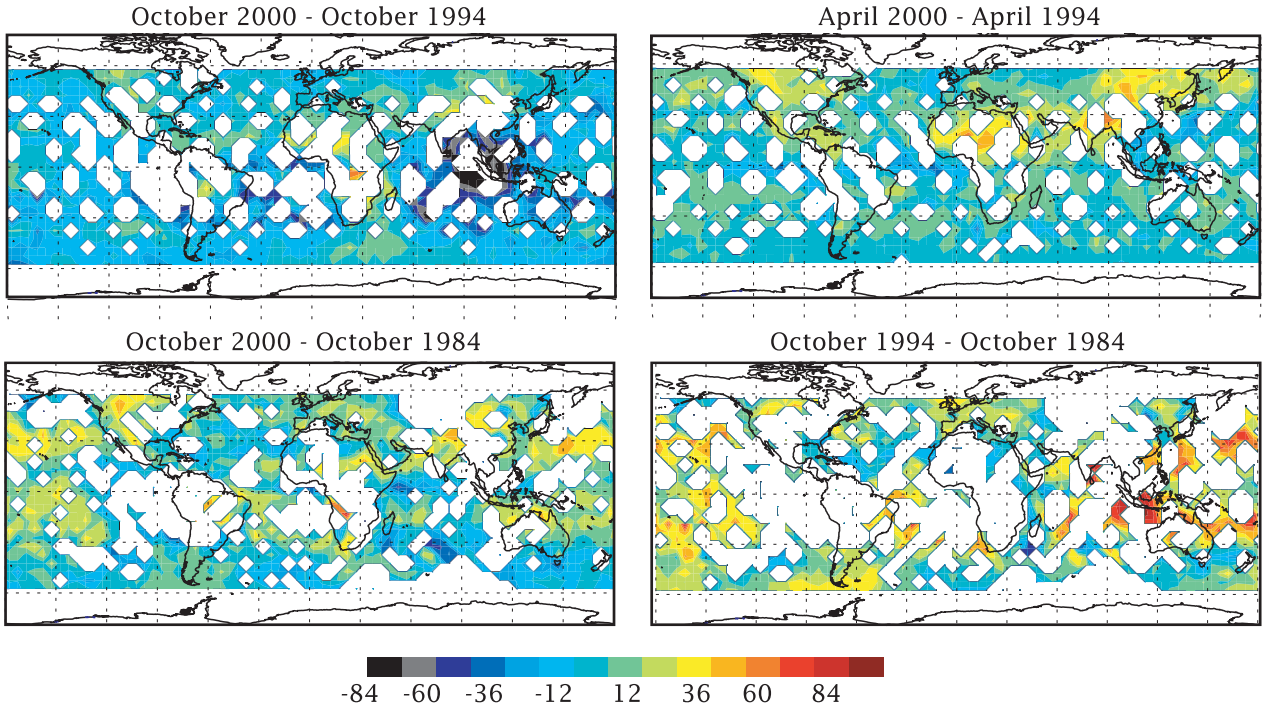

Figure 8. Differences in CO (ppbv) observed during different years from space corrected for the instruments' atmospheric sampling or viewing differences (except for the MAPS-to-MAPS comparison).

[30] Differences between the 1984, 1994 and 2000–2004 data sets are given in Table 5. All differences are computed using only points where data are present at both times. The October 2000–2004 versus 1994 values are also shown using the 1984 area masking for comparison with the other differences relative to 1984. This primarily affects southern Africa, where very little coverage is available during 1984 and we therefore subsequently disregard the 1984 comparisons there. We caution that there are certainly not enough data as a function of time to provide reliable trend estimates. However, distinct differences between the various years are apparent for some regions. The global mean difference between years is small during April. In October, 1994 observations show considerably more CO globally than 1984, while 2000–2004 falls about midway between 1984 and 1994 values. Much of the 1994 enhancement is probably due to the well-documented Indonesian fires that year.

[31] On a regional scale, South America follows the global October pattern of more CO during 1994 than either 1984 or 2000–2004, though the coverage is quite limited (Figure 8). October CO levels that are consistently high during 1994 and 2000–2004 relative to 1984 are seen over southeast Asia, North America and Europe. During April, the more than 12 ppbv greater 2000–2004 versus 1994 values over North America, northern Africa, and southeast Asia are the primary changes. Variability in emissions is likely larger during October, and consistent with this many October values in Table 5 exceed 15 ppbv. The larger of the differences shown in the table typically exceed the reported error relative to correlative measurements (3–10% of a mean value of ~85–120 ppbv) for the two instruments.

5. Sensitivity Studies

[32] To evaluate the potential causes of the variations seen during the different years of observations, several other sensitivity studies were run in addition to the BB00/E95 run introduced previously. These allowed us to test the influence

Table 5. Differences in CO Between Space-Based Measurements in Different Years[a]

Region	April 2000–2004 Mean –1994	October 2000–2004 Mean –1994	October 2000–2004 Mean –1994, 84 Masking	October 1994–1984	October 2000–2004 Mean – 1984
Global	2.4	−8.7	−8.8	18.9	9.2
N. America	12.6	2.6	2.5	12.9	13.3
S. America	−1.8	−16.1	−15.9	20.0	7.1
Europe	4.6	3.0	3.0	14.6	15.1
N. Africa	17.1	8.5	8.7	−4.9	8.0
S. Africa	4.6	10.3	0.1	−10.5	7.3
SE Asia	15.8	−0.1	4.6	27.4	28.7

[a]Differences are in ppbv. Data from 2000–2004 are from the MOPITT 500 hPa retrieval level, earlier data are from MAPS. Values have been adjusted for instrument viewing differences when the two instruments are compared (all columns except 1994–1984) using the viewing difference derived from the GCM control run. Values are quite similar (within 3.5 ppbv) using the viewing difference from the BB00/E95 run.

Table 6. Sensitivity Simulations

Name	Meteorology	Emissions
Control	GCM climate	1990 GEIA
MET	nudged	1990 GEIA
BB00	nudged	1990 GEIA except 2000–2001 biomass burning CO
75pctIND	nudged	1990 GEIA except 2000–2001 biomass burning CO and industrial CO at 75%
E95IND	nudged	1990 GEIA except industrial CO from EDGAR 1995
E95	nudged	1995 EDGAR
BB00/E95	nudged	1995 EDGAR except 2000–2001 biomass burning CO
33pctISOP	nudged	1995 EDGAR except 2000–2001 biomass burning CO and isoprene emissions at 33%

of the meteorology during 2000–2001 and of altered emissions from biomass burning, industrial sources, and isoprene (Table 6). The emissions were chosen to represent both a range of existing estimates and to best match conditions during the MOPITT phase 1 observations. These studies all used nudging toward assimilated meteorological fields and were all initialized with a 15 month spin-up. They began in January 1999, and we report only on April 2000 to April 2001. Methane emissions were unchanged in these runs from the control, however other hydrocarbon emissions were prescribed according to either GEIA or EDGAR, leading to variations in the indirect CO source from hydrocarbon oxidation. The runs are referred to hereafter by the names given in Table 6, which highlight the main perturbation imposed.

[33] Analyses of each of these runs were performed using the MAPS and MOPITT 2000 sampling. We focus on the regional changes in the area-weighted mean values and the regression coefficients to examine the response of both the amount and distribution of CO. These have been calculated by comparing each simulation to its control, which is another of the runs listed in Table 6 without the relevant perturbation but otherwise identical. Thus the runs have different controls from one another. This setup has the advantage of allowing us to examine simulations with more than one emission change relative to our standard control. For the mean values, we are interested only in the magnitude of the response to a particular emission or meteorology change, so all values shown are absolute values. Though the magnitude of emissions and meteorology changes in our runs does not necessarily span present uncertainties or variability, it is useful to gauge the sensitivity to particular perturbations. In some cases more than one perturbation to a particular source also gives an indication of how robust the response is. Regression coefficients and mean value sensitivities are shown in Figure 9. The regression coefficient and mean bias give an indication of the sensitivity of the spatial pattern and the overall mean value, respectively, to the imposed perturbation. The regression coefficient also indicates improvement as it increases (improvements to the mean value could be indicated by bias changes of either sign depending upon the initial bias value, hence only absolute values are shown). Area-weighted mean value changes derived from the space-based measurements accounting for the viewing difference between instruments (as given in Table 5) are included for comparison. For all regions, comparison of the response to the two different biomass burning emissions changes (BB00 versus MET, BB00/E95 versus E95) and the two different industrial perturbations (E95IND versus MET, 75pctIND versus BB00) show a consistent response per Tg CO emissions change (so these are not shown for simplicity).

[34] We discuss the sensitivities by region, highlighting the most important perturbations in each area on the basis of the results shown in Figure 9. Beginning with North America and Europe (top row), both the April and October results indicate that CO in these areas is strongly sensitive to industrial emissions and only mildly sensitive to other changes. While little variation was observed between 1994 and 2000–2004 over Europe during April, fairly large differences were seen over North America. The October results again show large changes over North America, and this time also over Europe, but in both cases between 1984 and the two later periods (which are similar to one another). The values in both seasons substantially exceed the response to any factor other than industrial emissions. The sensitivity studies thus suggest that the changes of $\sim$13 ppbv could be related to industrial emissions. However, the interannual variability during the 5 MOPITT years in these regions, especially over Europe during October, is larger than the responses seen in the sensitivity studies. In other regions the spread of results in the various sensitivity studies generally encompasses the observed variability, but the underestimate at northern middle to high latitudes suggests that variations in sources such as boreal burning may be much larger than the variation between the emissions data sets we used. Over North America during April, the sensitivity to biomass burning is only marginally smaller than the temporal change, as is the interannual variability during the 2000–2004 period. Furthermore, the temporal differences between 1994 and 2000–2004 are quite different in April than in October for North America, which may point to a seasonally varying source such as biomass burning rather than industry. However, it is also plausible that increased industrial emissions contributed to part or even most of the $\sim$13 ppbv 1994 to 2000–2004 April increase, and the October results show minimal change between these times owing to a reduction in biomass burning during 2000–2004 relative to the very high levels during 1994 which offsets the contribution of industrial increases. Thus industrial emissions could account for a large portion of the October 1984 to 2000–2004 increase, again of about 13 ppbv, consistent with the April value. Together, these factors suggest that a sizable portion of the changes over North America and Europe likely stem from some combination of industrial and biomass burning emission changes (perhaps upwind in Siberia as well as locally).

[35] Over North America and Europe, long-term measurements of surface CO are an additional potential source of information on temporal changes. Data are most abun-

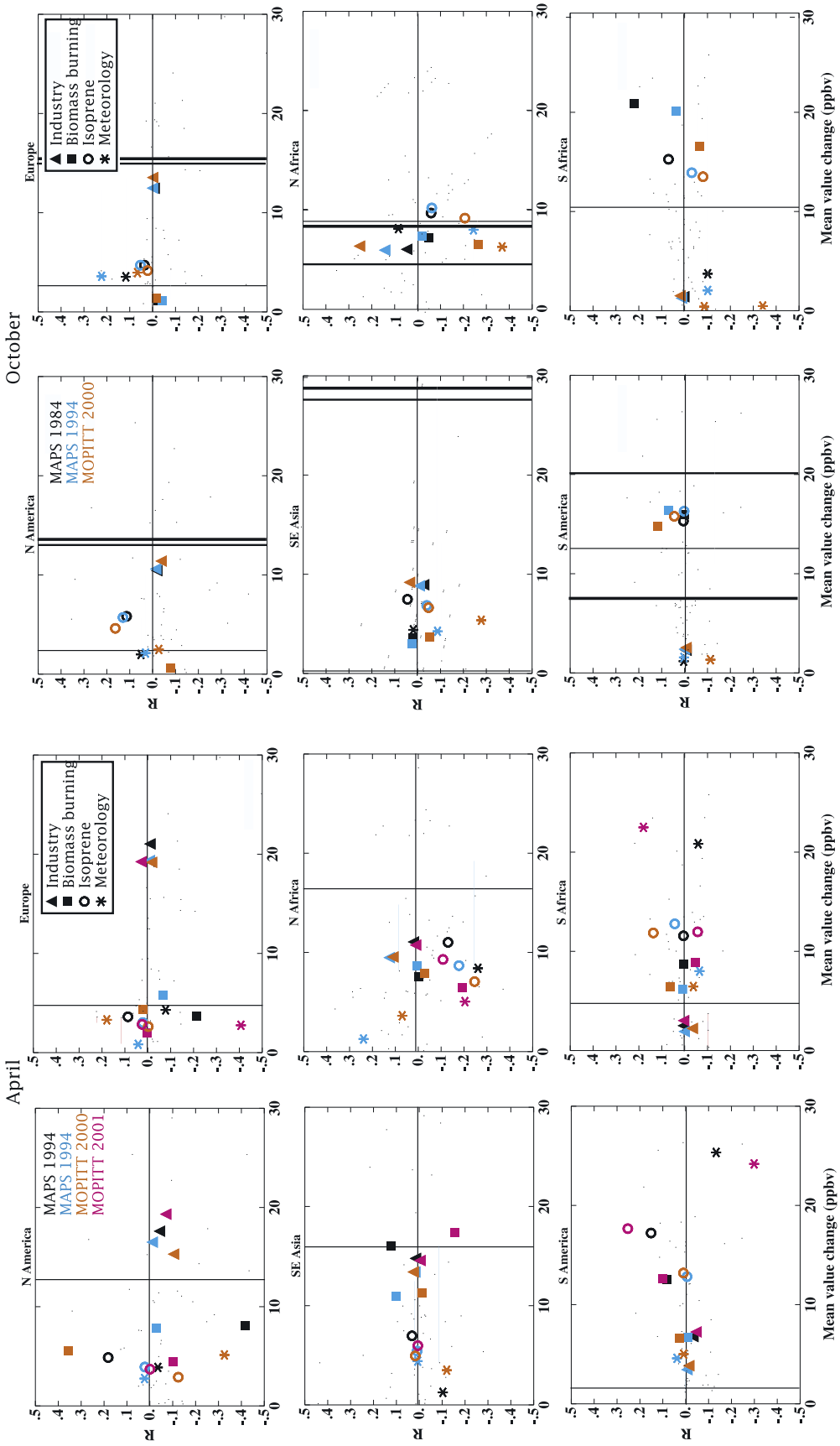
April
October
Europe
N America
N Africa
SE Asia
S America
S Africa
Industry
Biomass burning
Isoprene
Meteorology
MAPS 1994
MAPS 1994
MOPITT 2000
MOPITT 2001
MAPS 1984
MAPS 1994
MOPITT 2000
R
Mean value change (ppbv)

Figure 9

dant within the CMDL network for these regions [*Novelli et al.*, 1998]. An average of the six European sites during April shows 1994 values about 6 ppbv higher than the 2000–2002 average. As with the MOPITT/MAPS difference for this period, this value is well within interannual variability. Over North America, an average of 7–9 sites shows a decrease of 20 ppbv in 2000–2002 relative to 1994, quite different from the MOPITT/MAPS changes. The 1994 values were not particularly anomalous compared with neighboring years in the surface data set. However, the surface measurements are taken at rural locations and are largely reflective of local conditions in the boundary layer. In contrast, the satellites see mostly CO in the middle troposphere, reflecting sources over a wide region. They are thus inherently much more sensitive to the large emissions from polluted areas, making them difficult to compare with surface data from rural sites. October data are consistent with the satellites in showing considerably more variability than during April. In general, however, the space-based measurements provide a measure of CO reflective of pollution mixed over large spatial scales which is not comparable to the ground-based data.

[36] We now investigate sensitivities over southeast Asia (Figure 9, middle row), where 2000–2004 space-based observations showed substantially more April CO than 1994 (~16 ppbv). The sensitivity tests indicate that for this region, emissions from both biomass burning and industry could have been responsible. Even larger differences occur during October, but in this season CO is quite sensitive to industry, isoprene emissions, meteorology, and biomass burning emissions. The very large changes of ~27–29 ppbv between 1984 and the later years appear to require a contribution from several sources, most likely including industry. Note that the industrial emissions in most areas seem to have only a minor impact on the spatial pattern (as seen in the regression coefficients), while the biomass burning source affects this pattern more significantly. This suggests the potential for discrimination between sources based on long-term changes in the CO distribution.

[37] Northern Africa showed increases in CO levels of about 8–17 ppbv in both seasons between 1994 and 2000–2004, with little change during October between 1984 and 1994. In this region, CO values are sensitive to all the factors investigated (Figure 9, middle row), making any attribution of changes quite difficult. We believe this results from northern Africa's position just below a strong pollution gradient toward Europe which allows it to be affected by changes in European industrial emissions and in meteorology in addition to the local biomass burning and isoprene sources. Note that the reduced isoprene run shows a sizable reduction in the regression coefficient in all the cases, so that the spatial pattern, in addition to the mean value, points toward a larger isoprene source.

[38] Over South America and southern Africa (Figure 9, bottom row) large changes were seen in October that were not present in April. Both regions show large sensitivities to both biomass burning and isoprene emissions changes, and little response to meteorology or changes in industrial emissions. We note that South America, like southern Africa, had relatively sparse spatial coverage during 1984. However, the sensitivities shown in Figure 9 for the 1984 sampling (black) tend to be similar to those for the other samplings, suggesting that the coverage may not have greatly biased the results.

[39] The preceding region-based analysis revealed that CO in most areas is primarily sensitive to emissions changes. While typically of lesser importance, it is also interesting to examine the role of meteorological variations specifically. The April results include two sets of points comparing MAPS 1994 values with the model. For comparison with MOPITT we sampled the model during the year of the observations since these simulations used nudged meteorology, but for MAPS we sampled both 2000 and 2001 model years. The difference between these two MAPS versus model comparisons, for example over South America (black versus blue asterisks in Figure 9), indicates that the meteorology in some years looks quite similar to the model climatology, but not in others. Similar conclusions are drawn from sampling later MOPITT years (not shown). For example, over South America during April, changing from the GCM climatology to the 2001 meteorology has a large effect on the mean value and CO distribution (substantially worsening the regression coefficient), while the 2000 meteorology does little. The 2001 meteorology often has a noticeable effect, leading to a more realistic spatial pattern over southern Africa during April, but more typically to a less realistic one such as over Europe and North Africa. The October 2000 meteorology similarly leads to a less realistic distribution in most regions. The sensitivity to biomass burning over North America also appears to be strongly influenced by meteorology, as evidenced by the difference between the correlation coefficients for the 2 years compared with the same MAPS data. We note that the nudging toward meteorology indirectly affects the distribution of water vapor, soluble species, etc.,

Figure 9. Sensitivity of the regional CO spatial pattern and the area-weighted mean value to the indicated emissions and meteorology changes in the GCM. Sensitivity of the mean CO value and distribution are given by the changes in the bias (horizontal axis) and correlation (vertical axis) between the model and the space-based observations, respectively. Comparisons were made between GCM simulations sampled analogously with the observations to which they are compared. The observed changes with time from Table 5 are included as vertical lines. For April, these give the differences between observations taken in 2000–2004 and 1994. For October, they give the differences between 2000–2004 and 1994 (thin), 1994 and 1984 (medium) and 2000–2004 and 1984 (thick). All MOPITT-to-MAPS comparisons account for the viewing difference between the instruments based on the GCM control run (e.g., the top left plot is (MOPITT October 2000–2004 – MAPS October 1994) + (GCM October MAPS sampling – GCM October MOPITT sampling)). October differences over southern Africa relative to 1984 are not included owing to their sensitivity to the limited spatial coverage that year.

Table 7. Comparison of the CO Budget in This Study With Estimates From Inverse and Forward Models[a]

	This Work	Inverse Models				Forward Models	
		[*Pétron et al.*, 2004]	[*Arellano et al.*, 2004]	[*Pétron et al.*, 2002]	[*Bergamaschi et al.*, 2000]	[*Holloway et al.*, 2000]	[*Kanakidou et al.*, 1999]
Direct	845–1037	1228–1384	1313–1533	1528–1694	1347–1565	1048	1040–2362
Indirect	1148–1670	1640–1650	915–1002	1461–1536	1391–1653	1443	840–1459
Total	1993–2707	2878–3024	2228–2535	2960–3067	2867–3009	2491	1218–2742

[a]CO budget is in Tg/yr. Direct represents surface emissions of CO, while indirect represents chemical formation in the atmosphere by hydrocarbon oxidation. However, classification of emissions as either direct or indirect is not consistent across models depending on how emissions of volatile organic carbons (VOCs) are included. In the GISS model, for example, these are included explicitly so fall under indirect, leading to lower direct values than in some other studies that include VOC emissions as equivalent direct CO emissions.

in addition to directly changing dynamics, enabling impacts to occur via many pathways.

6. Discussion and Future Directions

[40] The analyses presented above provide indications of probable causes of temporal changes in CO amounts for several regions. Over the polluted regions of North America and Europe, biomass burning and industrial sources appear likely to be related to temporal changes. In line with expectations, large changes over South America and southern Africa during October are most plausibly accounted for by either biomass burning or isoprene emissions, or a combination of the two. CO over southeast Asia and northern Africa is sensitive to a variety of emissions and meteorology, making attribution generally more difficult in these areas. It seems likely that increases in industrial emissions made a substantial contribution to the very large changes over southeast Asia, however.

[41] The potential for understanding trends in tropospheric pollution using long-term space-based observations interpreted via a model to account for instrumental viewing differences appears great. Sampling two fairly different simulations demonstrated that the viewing difference was a relatively robust quantity. The changes in time are large enough to be distinguished above instrumental biases, interannual variability or uncertainties in the model-derived viewing difference. The present comparison is greatly limited, however, by the sparsity of available data. Especially prior to 2000, the data are limited in both spatial coverage (Figure 3) and temporal coverage (only April and October, and only 1984 and 1994).

[42] The modeling component is also limited by the uncertainties in CO emissions. While our studies used a fairly wide range of emissions, recent inverse and forward modeling studies show an even larger range of potential emissions (Table 7). Especially striking is that the most recent inverse studies using MOPITT data differ so sharply from one another [*Arellano et al.*, 2004; *Pétron et al.*, 2004]. This large uncertainty makes it difficult to know the magnitude of temporal changes in emissions that may have actually taken place.

[43] Nonetheless, the current study indicates that using models to aid in the interpretation of space-based observations from multiple instruments can provide significant new insights into tropospheric pollutants. For example, these results make a strong case that biomass burning contributed to enhanced levels of CO over South America during 1994 relative to 1984 or 2000–2004 and over southern Africa during 2000–2004 relative to 1994. Over southeast Asia, MOPITT observations indicate substantially greater pollution in April 2000–2004 than in 1994, and in October 2000–2004 and 1994 relative to 1984. These consistent increases at both times of year appear most likely associated with enhancements in both industrial emissions and biomass burning. Consistent increases in CO over northern Africa are also seen, though they appear potentially related to numerous factors. Given the large interannual variability revealed by the MOPITT data set, the analysis is clearly limited by the single years of data available during the 1980s and 1990s. However, the results provide tantalizing suggestions of the potential for global monitoring of tropo-

spheric pollutants from space, and suggest that with greater temporal and spatial coverage our understanding of temporal changes and factors governing those changes could be dramatically improved.

[44] **Acknowledgments.** This work was supported by NASA's Atmospheric Chemistry Modeling and Analysis Program (DTS, GF) and by NASA grant G04GO58G (LKE). The National Center for Atmospheric Research is operated by the University Corporation of Atmospheric Research under sponsorship of the National Science Foundation.

References

Arellano, A. F. J., P. S. Kasibhatla, L. Giglio, G. R. van der Werf, and J. T. Randerson (2004), Top-down estimates of global CO sources using MOPITT measurements, *Geophys. Res. Lett.*, *31*, L01104, doi:10.1029/2003GL018609.

Benkovitz, C. M., M. T. Scholtz, J. Pacyna, L. Tarrason, J. Dignon, E. C. Voldner, P. A. Spiro, J. A. Logan, and T. E. Graedel (1996), Global gridded inventories of anthropogenic emissions of sulfur and nitrogen, *J. Geophys. Res.*, *101*, 29,239–29,253.

Bergamaschi, P., R. Hein, M. Heimann, and P. J. Crutzen (2000), Inverse modeling of the global CO cycle: 1. Inversion of CO mixing ratios, *J. Geophys. Res.*, *105*, 1909–1928.

Connors, V. S., B. B. Gormsen, S. Nolf, and H. G. Reichle (1999), Space-borne observations of the global distribution of carbon monoxide in the middle troposphere during April and October 1994, *J. Geophys. Res.*, *104*, 21,455–21,470.

Deeter, M. N., et al. (2003), Operational carbon monoxide retrieval algorithm and selected results for the MOPITT instrument, *J. Geophys. Res.*, *108*(D14), 4399, doi:10.1029/2002JD003186.

Deeter, M. N., L. K. Emmons, D. P. Edwards, J. C. Gille, and J. R. Drummond (2004), Vertical resolution and information content of CO profiles retrieved by MOPITT, *Geophys. Res. Lett.*, *31*, L15112, doi:10.1029/2004GL020235.

Emmons, L. K., et al. (2004), Validation of Measurements of Pollution in the Troposphere (MOPITT) CO retrievals with aircraft in situ profiles, *J. Geophys. Res.*, *109*, D03309, doi:10.1029/2003JD004101.

Faluvegi, G., K. Alapaty, H. G. Reichle, R. Mathur, S. Raman, and V. S. Connors (1999), Simulation of carbon monoxide transport during April 1994, *J. Geophys. Res.*, *104*, 21,471–21,485.

Fung, I., J. John, J. Lerner, E. Matthews, M. Prather, L. P. Steele, and P. J. Fraser (1991), Three-dimensional model synthesis of the global methane cycle, *J. Geophys. Res.*, *96*, 13,033–13,065.

Gettelman, A., J. R. Holton, and K. H. Rosenlof (1997), Mass fluxes of O_3, CH_4, N_2O, and CF_2Cl_2 in the lower stratosphere calculated from observational data, *J. Geophys. Res.*, *102*, 19,149–19,159.

Holloway, T., H. Levy II, and P. S. Kasibhatla (2000), Global distribution of carbon monoxide, *J. Geophys. Res.*, *105*, 12,123–12,148.

Kanakidou, M., et al. (1999), 3D global simulations of tropospheric CO distributions: Results of the GIM/IGAC intercomparison 1997 exercise, *Chemosphere Global Change Sci.*, *1*, 263–282.

Koch, D., D. Jacob, I. Tegen, D. Rind, and M. Chin (1999), Tropospheric sulfur simulation and sulfate direct radiative forcing in the Goddard Institute for Space Studies general circulation model, *J. Geophys. Res.*, *104*, 23,799–23,822.

Logan, J. A. (1999), An analysis of ozonesonde data for the troposphere: Recommendations for testing 3-D models and development of a gridded climatology for tropospheric ozone, *J. Geophys. Res.*, *104*, 16,115–16,149.

Novelli, P. C., K. A. Masarie, and P. M. Lang (1998), Distributions and recent changes in carbon monoxide in the lower troposphere, *J. Geophys. Res.*, *103*, 19,015–19,034.

Olivier, J. G. J., and J. J. M. Berdowski (2001), Global emissions sources and sinks, in *The Climate System*, edited by J. Berdowski et al., pp. 33–78, A. A. Balkema, Brookfield, Vt.

Pétron, G., C. Granier, B. Khattatov, J.-F. Lamarque, V. Yudin, J.-F. Müller, and J. Gille (2002), Inverse modeling of carbon monoxide surface emissions using Climate Monitoring and Diagnostics Laboratory network observations, *J. Geophys. Res.*, *107*(D24), 4761, doi:10.1029/2001JD001305.

Pétron, G., C. Granier, B. Khattatov, V. Yudin, J.-F. Lamarque, L. Emmons, J. Gille, and D. P. Edwards (2004), Monthly CO surface sources inventory based on the 2000–2001 MOPITT satellite data, *Geophys. Res. Lett.*, *31*, L21107, doi:10.1029/2004GL020560.

Prinn, R. G., et al. (2001), Evidence for substantial variations of atmospheric hydroxyl radicals in the past two decades, *Science*, *292*, 1882–1888.

Reichle, H. G., et al. (1999), Space shuttle based global CO measurements during April and October 1994, MAPS instrument, data reduction, and data validation, *J. Geophys. Res.*, *104*, 21,443–21,454.

Schmidt, G. A., et al. (2005), Present day atmospheric simulations using GISS ModelE: Comparison to in-situ, satellite and reanalysis data, *J. Clim.*, in press.

Shindell, D. T., J. L. Grenfell, D. Rind, C. Price, and V. Grewe (2001), Chemistry-climate interactions in the Goddard Institute for Space Studies general circulation model: 1. Tropospheric chemistry model description and evaluation, *J. Geophys. Res.*, *106*, 8047–8076.

Shindell, D. T., G. Faluvegi, and N. Bell (2003), Preindustrial-to-present-day radiative forcing by tropospheric ozone from improved simulations with the GISS chemistry-climate GCM, *Atmos. Chem. Phys.*, *3*, 1675–1702.

Shindell, D. T., G. Faluvegi, N. Bell, and G. A. Schmidt (2005), An emissions-based view of climate forcing by methane and tropospheric ozone, *Geophys. Res. Lett.*, *32*, L04803, doi:10.1029/2004GL021900.

Van der Werf, G. R., J. T. Randerson, G. J. Collatz, and L. Giglio (2003), Carbon emissions from fires in tropical and subtropical ecosystems, *Global Change Biol.*, *9*, 547–562.

L. K. Emmons, National Center for Atmospheric Research, Boulder, CO 80307, USA.

G. Faluvegi, Center for Climate Systems Research, Columbia University, New York, NY 10027, USA.

D. T. Shindell, NASA Goddard Institute for Space Studies, New York, NY 10025, USA. (dshindell@giss.nasa.gov)